2024, 21(4): 1391-1402
https://doi.org/10.21123/bsj.2023.8117
P-ISSN: 2078-8665 - E-ISSN: 2411-7986
Baghdad Science Journal

A selective NH_3 gas sensor based on $(Ag_2O)_{1-x}(SnO_2)_x$ nanocomposites thin films at various operating temperatures

Nada Mohammed Abas, Anwar Ali Baqer*

Department of Physics, College of Science for Women, University of Baghdad, Baghdad, Iraq
*Corresponding Author.

Received 26/11/2022, Revised 27/03/2023, Accepted 29/03/2023, Published Online First 20/09/2023, Published 01/04/2024

Abstract

The pulsed laser deposition (PLD) technique was used to prepare the $(Ag_2O)_{1-x}(SnO_2)_x$ nanocomposite thin films with different ratios of x=0, 0.2 and 0.4wt and deposited on glass substrates. The films were subsequently annealed in the air for two hours at 300 °C. The $(Ag_2O)_{1-x}(SnO_2)_x$ nanocomposite was confirmed to have formed by the x-ray diffraction (XRD) investigation. According to field emission scanning electron microscopy (FESEM), the created $(Ag_2O)_{1-x}(SnO_2)_x$ particles were spherical in shape. Energy Dispersive X-Ray Analysis (EDX) is used to confirm the elements in composite films. Atomic Force Microscopy (AFM) analysis shows that the produced films had grains size between 37.68 - 49.57nm and root mean square (RMS) roughness of 4.92-8.22nm. The prepared films have a direct energy gap between 2.06 and 3.36 eV, according to UV-visible (UV-Vis) spectrometer data. The films have been tested for NH_3 sensing under various operating temperatures. The observed variations in the gas sensing response's thin film resistance are suggestive of either n-type or p-type conductivity. When reducing gas is present, the resistance of $(Ag_2O)_{1-x}(SnO_2)_x$ films increases when x=0, 0.2wt , indicating that the films are p-type, however, the thin film exhibits the reverse behavior at x=0.4wt, indicating that it is n-type. Additionally, all films produced showed a significant sensitivity to NH_3 gas at 95 ppm concentration. The Ag_2O thin film had a sensitivity of 50.5% at an operating temperature of 200°C with response and recovery times of 22.5 and 39.6 seconds, respectively. Furthermore, composite thin films showed greater sensitivity than pure silver oxide thin films.

Key words: Ag_2O- SnO_2, Nanocomposites, NH_3 gas sensor, Operating temperatures, Pulsed laser deposition.

Introduction

Ammonia (NH_3) is a very hazardous, flammable chemical gas that's widely used in the food-processing, pharmaceutical, and chemical sectors. These systems could leak, posing health risks. The detection of NH_3 in traces is crucial for industrial production, environmental safety, and human health[1]. Utilizing metal oxide semiconductor (MOSs) nanoparticles as the foundation of the sensor is an impressively effective way to increase the reaction speed, sensitivity, and selectivity of gas detecting characteristics. Researchers have conducted numerous works and investigated a variety of sensitive materials with the goal of understanding the sensing of NH_3 at room temperature [2-7]. One of many MOSs. Ag_2O is a p-type semiconductor with a direct band gap of 1.2 eV

2024, 21(4): 1391-1402
https://doi.org/10.21123/bsj.2023.8117
P-ISSN: 2078-8665 - E-ISSN: 2411-7986
Baghdad Science Journal

because of its stability, non-toxicity, low cost and sensitivity to gases, it is a preferred material for use in gas sensors[8-10]. Additionally, optoelectronic applications can make use of silver oxides [11-13]. In the mechanics of conduction, the oxygen vacancies in silver oxide are crucial[14]. Tin dioxide (SnO_2), an n-type wide band gap semiconductor (E_g = 3.6 eV) has been widely utilized in the detection of ammonia [15-16].

Recently, surface modification, doping, and the blending of semiconducting metal oxides have increased the sensitivity and selectivity of nanomaterials for semiconductor oxides. Depending on the kind of oxides and the type of reactive gas, the mixing procedure of oxides impacts the sensitivity and selectivity features. Due to changes in the surface of the manufactured composite, a particular mixture can yield good properties of one gas and poor properties of another[17]. Due to the improved gas-sensing performance of n-type oxides and p-type semiconductor oxides toward target gases, this combination has received a lot of attention, such as producing a nanocomposite from the mixture of n-typeIn$_2$O$_3$/p-type CuO by the chemical spray pyrolysis process to improve NO_2 gas sensor applications[17], Low-concentration NO_2 gas sensing using n-type TiO_2/p-type Ag_2O composite nanorods made using the sputtering decoration process[18], To fulfill the needs for low-level acetone detection, a gas sensor based on n-type ZnO/p-type CuO composite nanostructure (ZCS) has been developed[19].

However, the composite p-type Ag_2O/n-type SnO_2 for sensor application has only been examined by a small number of researchers such as Yang and co-workers was reported to enhance H_2S-sensing capability, nanocasting was used to create mesoporous Ag_2O/SnO_2[20]. For applications in H_2 gas detection, SnO_2/Ag_2O ceramic nanocomposite (CNP) was created using the sol-gel process was studied by Rizi and co-workers[21]. Sputtering techniques and co-sputtering, respectively, are used to create monolayer and two-layer n-type SnO_2/p-type Ag_2O composite thin films for NO_2 gas sensor applications were explored by Liang and co-workers[22]. Thus, further research is still necessary.

In this study, we used pulse laser deposition (PLD) to create an $(Ag_2O)_{1-x}(SnO_2)_x$ nanocomposite. The impact of composition variations of $(Ag_2O)_{1-x}(SnO_2)_x$ on structural morphology, compositional, and optical features are investigated using XRD, FESEM, AFM, EDX, and UV-Vis analysis. Further research was done on the ammonia gas detecting behaviors of synthesized films at various operating temperatures and the effects of varying ratios of x (0, 0.2, and 0.4wt), compared to pure Ag_2O sample. As a result, the main objective of this research is to enhance the gas sensitivity for NH_3 of based on $(Ag_2O)_{1-x}(SnO_2)_x$ nanoscale sensors at low temperatures.

Materials and Methods

Ag_2O and SnO_2 powders were combined in various ratios of x= 0,0.2, and 04wt using a hydraulic piston, the mixtures were crushed into pellets measuring 25 mm in diameter and 4 mm in thickness. These pellets were sintered for one hour at 100 ºC. The deposition was carried out using a turbo rotary pump at 2 10^{-3} mbar.

All pellets were exposed to radiation using a 532 nm Q-switched Nd: YAG laser (Model HF-301, Huafei Technology, China) operating at 300 mJ and 300 laser pulses per second (6 Hz) with a pulse width of 10 ns. The thickness of the thin films was around 200±10 nm. Nanocomposite thin film preparation is completed by annealing films at 300 °C for 2 hours.

The Tolansky interferometer technique is used to measure a thin film thickness. The UV/Visible Spectrophotometer SP-8001, manufactured by Metertech in Taiwan, was used to measure the samples' optical characteristics. By analyzing the XRD pattern produced by the Philips X-ray diffractometer model PW 1710 (= 1.5405 Å for Cu K), the structural characterization of the samples was completed. Energy Dispersive X-Ray (EDX) Analyses and the SUPRA 55 VP field emission scanning electron microscope (FESEM) were used to evaluate the materials' surface morphology and elemental analysis. Through the use of an atomic force microscope (AFM) in tapping mode, the grain size and surface roughness are examined. Finally, the synthesized composite film's sensitivity to NH_3 gas was tested at various Ag_2O ratios and different operating temperatures.

2024, 21(4): 1391-1402
https://doi.org/10.21123/bsj.2023.8117
P-ISSN: 2078-8665 - E-ISSN: 2411-7986
Baghdad Science Journal

Results and Discussion

XRD analysis

Fig. 1 shows the x-ray diffraction patterns of $(Ag_2O)_{1-x}$ $(SnO_2)_x$ composite thin films deposited on glass substrate at different ratios (x= 0, 0.2 and 0.4wt) , which were obtained by pulsed laser deposition and annealed at 300 ºC for two hours.

Fig 1a shows typical peaks that correspond to the trigonal (hexagonal axis) Ag_2O (011) and (004) peaks positioned at 2θ =38.16° and 77.5° respectively (PDF card no. 96-150-9685)[23]. In addition, it can be seen that Ag_2O has been deposited alongside the elements Ag and another oxide AgO, which are present at 2θ = 44.36° and 64.53°, respectively. However, compared to other materials, Ag_2O exhibits a greater peak of hexagonal crystal lattice along the orientation (011). The quality of the crystal structure is represented by the quality of the XRD peaks; a more intense peak of Ag_2O denotes better crystallinity[24].

Moreover, the mixed tetragonal structure of SnO_2 can be shown in Figs b and c, based on the diffraction peaks (110), (101) that are situated at 2θ = 26.62° and 33.94°, respectively. (JCPDS 01-077-0447)[25-26] with Ag_2O's hexagonal structure provided evidence that an Ag_2O-SnO_2 nanocomposite had formed. Moreover, it is noted that the peak intensities of the tetragonal SnO_2 increased as the ratio of SnO_2 increased from 0.2 to 0.4wt, indicating a reduction in the degree of crystallization of the hexagonal structure Ag_2O[27].

Based on the Scherrer equation below, the average crystallite size of nanocomposite $(Ag_2O)_{1-x}$ $(SnO_2)_x$ thin films was calculated for all peaks[25]:

$$D = K\,\lambda / \beta \cos\theta \quad \ldots\ldots\ldots\ldots\ldots\ldots \; 1$$

where D is crystallite size, k is a constant (0.9), λ the X-ray wavelength 1.5418 Å, θ is Bragg's diffraction angle and β is the angular line width of half maximum intensity. XRD results shown in Table 1.

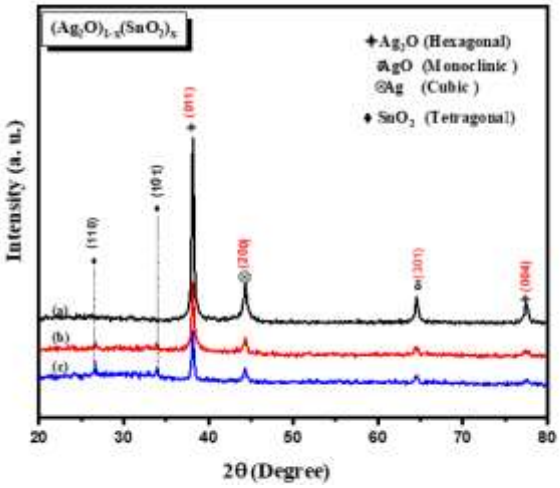

Figure 1. XRD patterns for the various ratios of the prepared films $(Ag_2O)_{1-x}$ $(SnO_2)_x$ nanocomposite.

Table 1. XRD characteristics for the $(Ag_2O)_{1-x}$ $(SnO_2)_x$ nanocomposite films that are prepared at various ratios.

Sample $(Ag_2O)_{1-x}$ $(SnO_2)_x$	2θ (Deg.)	dhkl (Å)	FWHM (Deg.)	hkl	Phase	C.S (nm)	Average C.S (nm)
	38.161	2.358	0.3938	(011)	Hexagonal (Ag_2O)	21.3487	
	44.3571	2.042	0.3936	(200)	Cubic (Ag)	21.787	
X=0	64.5761	1.44	0.3936	(301)	Monoclinic (AgO)	23.866	
Pure Ag_2O	77.5447	1.230	0.48	(044)	Hexagonal (Ag_2O)	21.220	22.055
	26.624	3.348	0.2952	(110)	Tetragonal (SnO_2)	27.643	
	33.941	2.641	0.2952	(101)	Tetragonal (SnO_2)	28.125	
	38.149	2.359	0.3936	(011)	Hexagonal (Ag_2O)	21.347	
X=0.2	44.367	2.041	0.3936	(200)	Cubic (Ag)	21.788	21.49
	64.53	1.444	0.5904	(301)	Monoclinic (AgO)	15.907	
	77.44	1.231	0.72	(004)	Hexagonal Ag_2O	14.137	
	26.624	3.348	0.2932	(110)	Tetragonal (SnO_2)	27.832	
	33.941	2.641	0.2948	(101)	Tetragonal (SnO_2)	28.164	
X=0.4	38.149	2.359	0.3927	(011)	Hexagonal (Ag_2O)	21.396	
	44.367	2.041	0.3936	(200)	Cubic (Ag)	21.788	21.54
	64.53	1.444	0.5904	(301)	Monoclinic (AgO)	15.907	
	77.44	1.231	0.72	(004)	Hexagonal (Ag_2O)	14.137	

2024, 21(4): 1391-1402
https://doi.org/10.21123/bsj.2023.8117
P-ISSN: 2078-8665 - E-ISSN: 2411-7986
Baghdad Science Journal

AFM analysis

When x=0, 0.2, and 0.4wt, $(Ag_2O)_{1-x}(SnO_2)_x$ nanocomposite AFM photos are displayed in Fig 2. The outcomes demonstrate that the films are nanocrystal line and have a rough surface. Ag_2O has a root mean square (RMS) roughness of 4.92 nm and grain size of about 41.98 nm (Fig 2a). Additionally, it is found that when x=0.2 and 0.4wt with high roughness, grain size is reduced for the $(Ag_2O)_{1-x}(SnO_2)_x$ nanocomposite thin film sensor structure, which is recognized to be crucial for achieving improved gas sensing response characteristics (Figs. 2b and c)[28-29]. AFM results are displayed in Table 2.

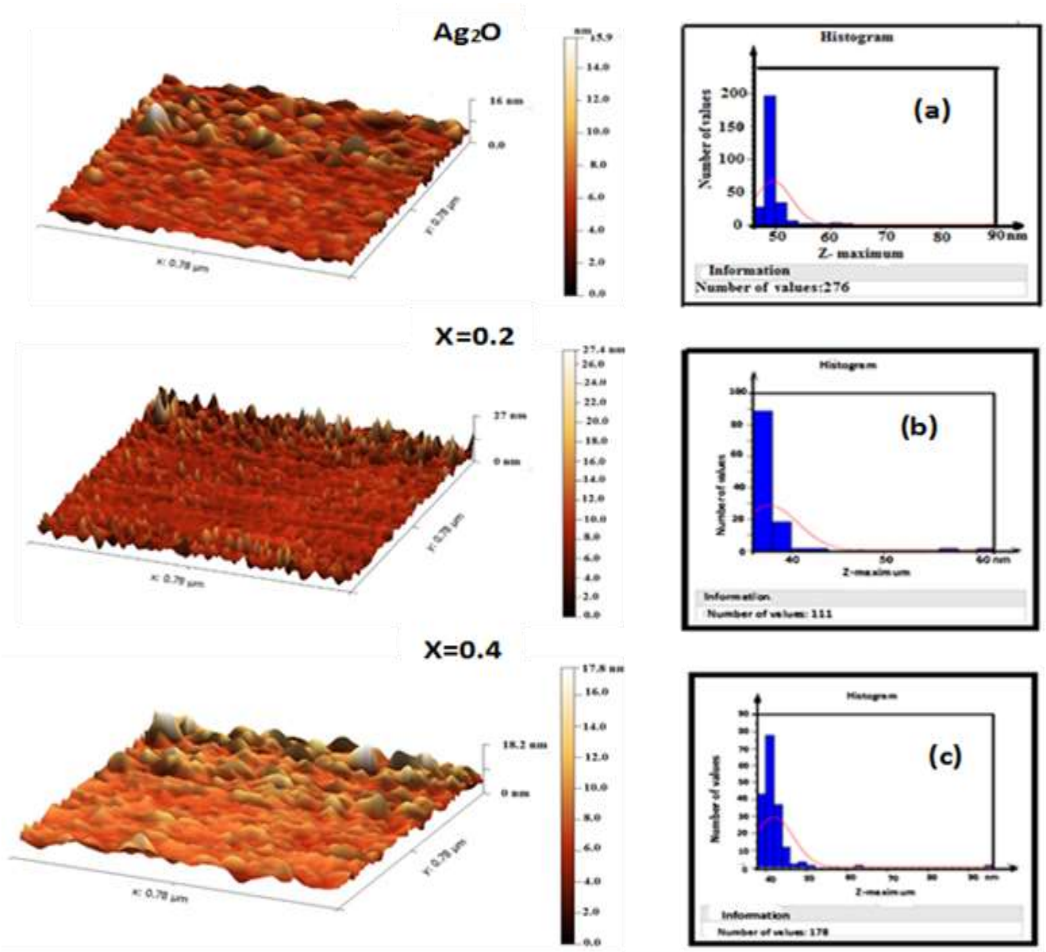

Figure 2. AFM images for the prepared films $(Ag_2O)_{1-x}(SnO_2)_x$ nanocomposite at various ratios and their granularity cumulating distribution.

Table 2. AFM parameters for the prepared $(Ag_2O)_{1-x}(SnO_2)_x$ nanocomposite films at various ratios, including Grainsize, Roughness average, and RMS roughness.

$(Ag_2O)_{1-x}(SnO_2)_x$	Grain size (nm)	Roughness Ave. (nm)	RMS Roughness (nm)
x=0 pure Ag_2O	41.98	3.813	4.92
x=0.2	37.68	6.157	8.22
x=0.4	49.57	4.294	5.17

FESEM analysis

Fig. 3 shows FESEM micrographs of $(Ag_2O)_{1-x}(SnO_2)_x$ films made by the PLD method. These films are made up of spherical nanoparticles. Using the software Image J, the average diameters of $(Ag_2O)_{1-x}(SnO_2)_x$ nanocomposite particles were estimated which were 15.92, 13.33, and 15.77 nm when x = 0, 0.2 and 0.4wt respectively.

When x=0.2wt as, the $(Ag_2O)_{1-x}(SnO_2)_x$ films include modest amounts of smaller nanoparticles

2024, 21(4): 1391-1402
https://doi.org/10.21123/bsj.2023.8117
P-ISSN: 2078-8665 - E-ISSN: 2411-7986
Baghdad Science Journal

with regular shapes. As a consequence raising the ratio of x causes the mean diameter of the nanoparticles to grow, which is consistent with AFM and XRD results.

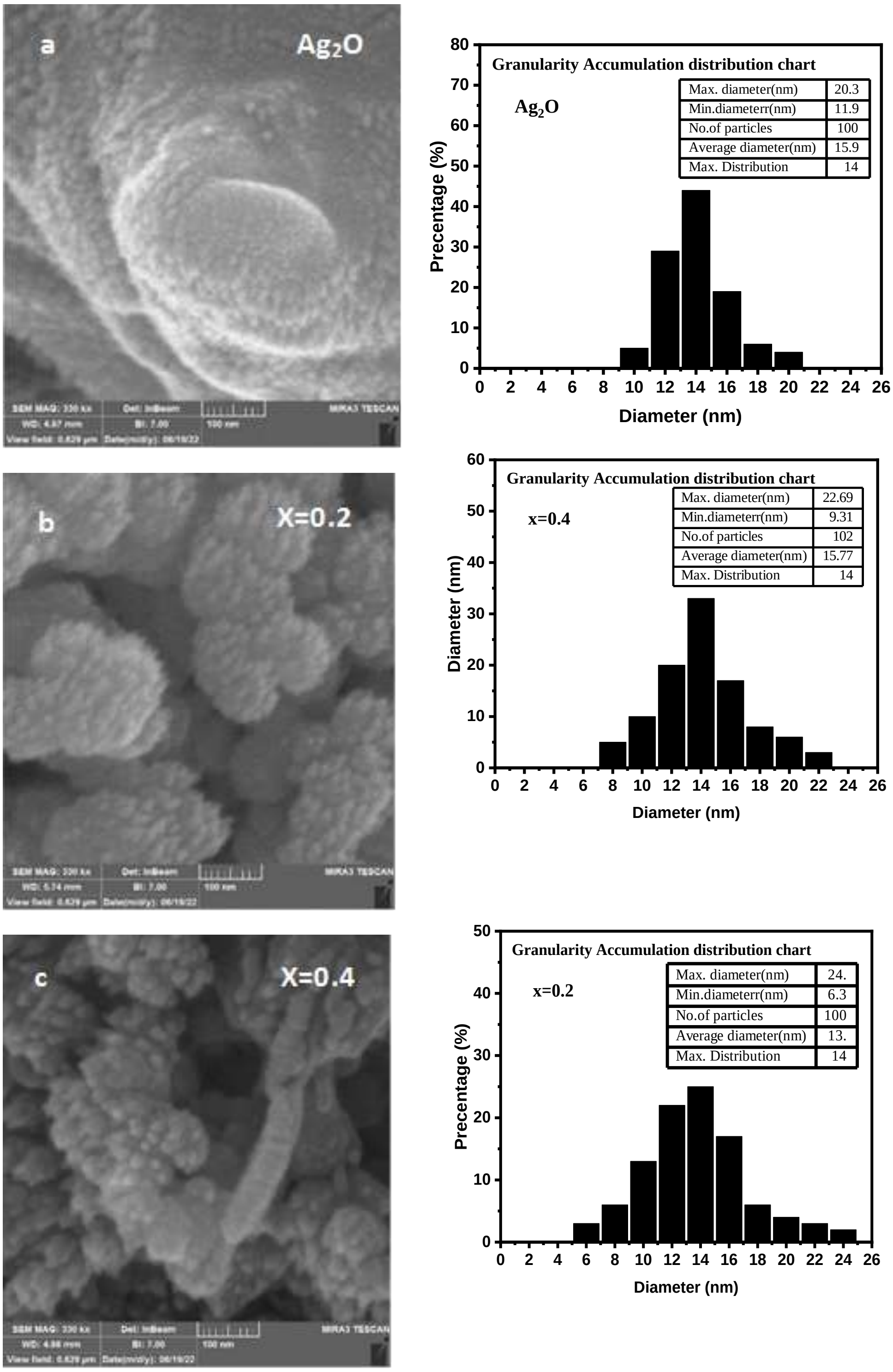

Figure 4. Field emission scanning electron microscopy images for the prepared films $(Ag_2O)_{1-x}(SnO_2)_x$ nanocomposite at various ratios

2024, 21(4): 1391-1402
https://doi.org/10.21123/bsj.2023.8117
P-ISSN: 2078-8665 - E-ISSN: 2411-7986
Baghdad Science Journal

EDX Analysis

The prepared samples' elemental composition was investigated using EDX analysis, with the findings shown in Fig 4.

Fig 4a the area has strong and weak peaks for oxygen and silver atoms, respectively, according to the EDX study. The development of silver oxide is indicated by the extremely low oxygen signal[30].

The EDX spectra of $(Ag_2O)_{1-x}(SnO_2)_x$ at x=0.2 and 0.4wt, respectively, are shown in Figs 4b and c, confirm the existence of the tin, silver, and oxygen elements that make up their composites. Additionally, it was discovered that Sn peak intensities increase with increasing the ratio of x, whereas Ag peak intensities in EDX spectrum data decrease, indicating the successful incorporation of SnO_2 into the composites. Table 3 lists the elements that have been found, together with their atomic and weight percentages, for all samples.

The peak at 2.12 keV is the distinctive peak of Au that can be seen in all samples that have been coated with Au in order to improve picture resolution using a FESEM instrument. In contrast, the glass substrate's Si characteristic peak lies at a wavelength of roughly 1.7 keV.

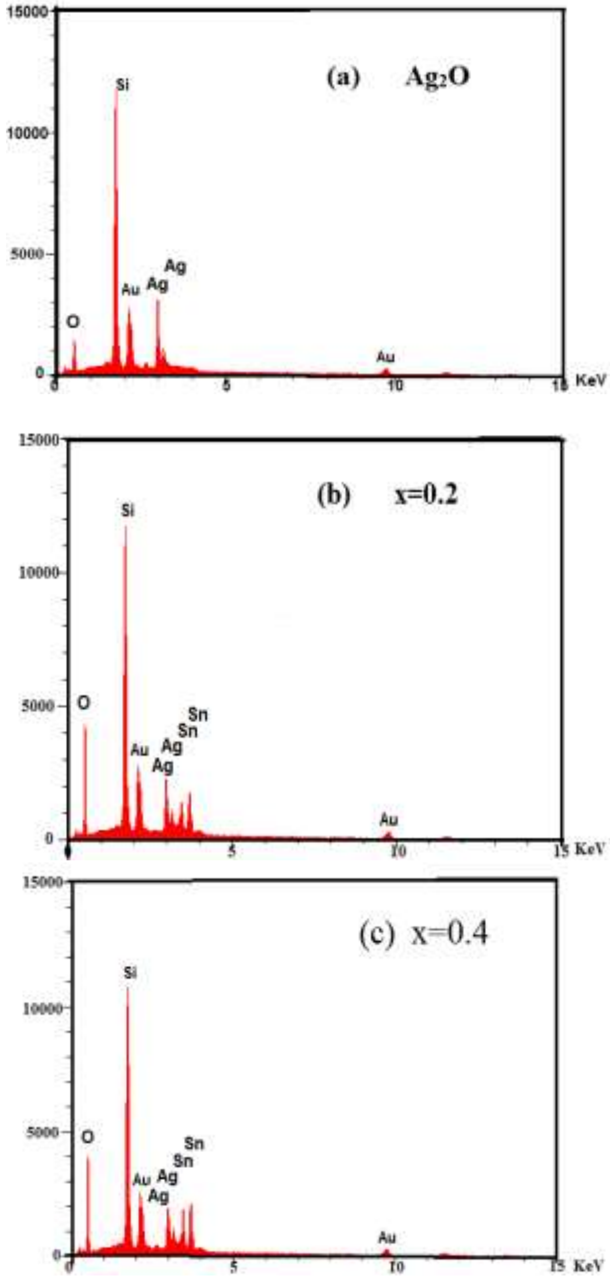

Figure 4. EDX spectra for the prepared films of $(Ag_2O)_{1-x}(SnO_2)_x$ nanocomposite at various ratios.

Table 3. EDX results for the prepared films of $(Ag_2O)_{1-x}(SnO_2)_x$ nanocomposite at various ratios.

Samples $(Ag_2O)_{1-x}(SnO_2)_x$	Elements	Wight %	Atomic %
Ag_2O	O	11.43	40.16 (1)
	Ag	88.57	49. 84
X=0.2	O	24.15	64.28
	Sn	31.57	17.46
	Ag	68.43	18.26
X=0.4	O	23.75	62.54
	Sn	45.84	17.27
	Ag	54.16	20.19

2024, 21(4): 1391-1402
https://doi.org/10.21123/bsj.2023.8117
P-ISSN: 2078-8665 - E-ISSN: 2411-7986

UV-Visible analysis

When x=0, 0.2, and 0.4wt, the $(Ag_2O)_{1-x}(SnO_2)_x$ nanocomposites' absorption behavior was examined using UV-visible spectroscopy. The normalized absorption spectra of $(Ag_2O)_{1-x}(SnO_2)_x$ nanocomposites, which were recorded at room temperature in the wavelength range of 300-800 nm, are shown in Fig 5.

It is clear from Fig 5a that in Ag_2O nanostructures, the absorption edge arises at 385 nm. As a result, the Ag_2O thin film's absorption edges show a blue-shift relative to their bulk, which is explained by the quantum confinement effect[31]. The absorption edges of $(Ag_2O)_{1-x}(SnO_2)_x$ nanocomposites for x=0.2 and 0.4wt were also nearly shifted to 375 and 366 nm, respectively, as illustrated in Figs 5b and c. According to the UV-Vis absorption spectra, the optical absorption edges of the $(Ag_2O)_{1-x}(SnO_2)_x$ nanocomposite shift towards a lower wavelength area with an increasing weight ratio of SnO_2. As a result, when compared to Ag_2O nanostructures, the blue shifts appeared in $(Ag_2O)_{1-x}(SnO_2)_x$ nanocomposites.

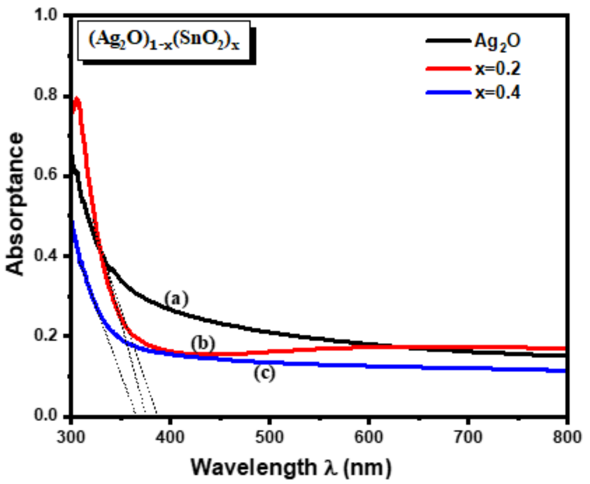

Figure 5. Shows the variation in absorption with wavelength for the prepared $(Ag_2O)_{1-x}(SnO_2)_x$ nanocomposite films at various ratios.

The Tauc plots for the $(Ag_2O)_{1-x}(SnO_2)_x$ nanocomposite is shown in Fig. 6 and were created using the appropriate UV-visible absorbance data. The relation: nanocomposites were used to build these charts.

$$\alpha h\nu = A(h\nu - Eg)^{1/2} \ldots\ldots\ldots\ldots 2$$

Where hν is the energy of a photon, A is a constant, and Eg is the optical band gap. Plotting the square of the optical absorption coefficient as a function of photon energy and extrapolating the linear region to the energy axis allows us to calculate the optical band gap values from Eq 2, as shown in Fig 6. When x=0, 0.2, and 0.4wt, respectively, the obtained energy band gap values are 2.06eV for Ag_2O film and 3.24 and 3.36eV for $(Ag_2O)_{1-x}(SnO_2)_x$ nanocomposites[32-33].The band gap energy of $(Ag_2O)_{1-x}(SnO_2)_x$ nanocomposites shifted to ~~the~~ blue due to the reduction in particle size compared to pure Ag_2O thin film [24].

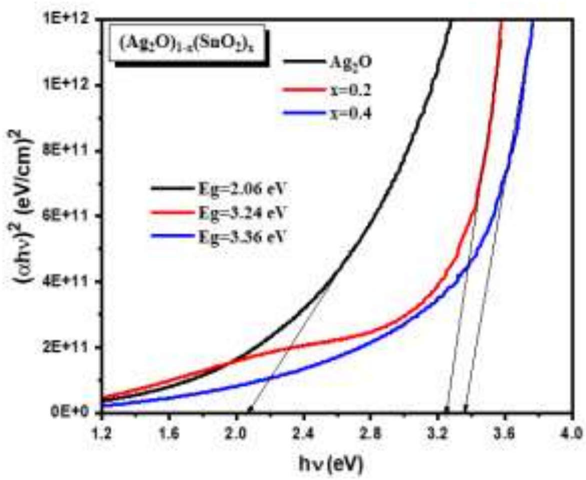

Figure 6. The relationship between $(\alpha h\nu)^2$ and photon energy (hν) for prepared$(Ag_2O)_{1-x}(SnO_2)$ nanocomposite films at various ratios.

Gas Sensor analysis

The reactions between semiconductor and atmospheric gases, which result in a change in the semiconductor resistance, are the basis for the semiconductor's sensing abilities. Adsorption of gases at the surface is the process that causes a change in conductivity. At first, oxygen in the air adsorbs and pulls electrons out of the semiconductor's conduction band. There are numerous potential processes that can happen when the desired gas concentration is injected. For an n-type semiconductor, the resistivity rises due to electron capture by an oxidizing gas and falls with the presence of a reducing gas due to electron

2024, 21(4): 1391-1402
https://doi.org/10.21123/bsj.2023.8117
P-ISSN: 2078-8665 - E-ISSN: 2411-7986

transfer into the conduction band, whereas the opposite is true for a p-type semiconductor[34].

Gas sensing are described in terms of the dynamic change in resistance and the gas-sensing response. For p-type semiconductors, the response is defined as the ratio of change in resistance, R /Ra; for n-type semiconductors, R/Rg, where Ra and Rg represent the resistance in air and the resistance when the gas is present respectively [7].

The dynamic variation in conductance caused by the insertion of gas pulses was used to determine the gas-sensing response, which was then displayed against various temperatures. Figs 7 to 9 shows the dynamic response of $(Ag_2O)_{1-x}(SnO_2)_x$ thin films at various temperatures between 80 and 250 °C toward 95 ppm of NH_3 gas (at gas-on shown by blue arrow and gas-off shown by red arrow). When exposed to reducing gas, the resistances of the $(Ag_2O)_{1-x}(SnO_2)_x$ thin film with x=0 and 0.2wt rise, showing the behavior of a p-type semiconductor. The behavior of x=0.2wt is not noticeably different from the behavior of the pure Ag_2O thin film. However, when exposed to reducing gas, the resistance of the $(Ag_2O)_{1-x}(SnO_2)_x$ thin film with x=0.4wt decreases, indicating n-type semiconductor characteristics. It is obvious that the p-type $(Ag_2O)_{1-x}(SnO_2)_x$ thin film, when x=0.2wt, has a substantially stronger gas sensing response with a shorter response and recovery time than the pure Ag_2O thin film and when x=0.4wt. Additionally, it is evident that between x=0.2 and 0.4wt, Ag_2O thin films' resistance increases.

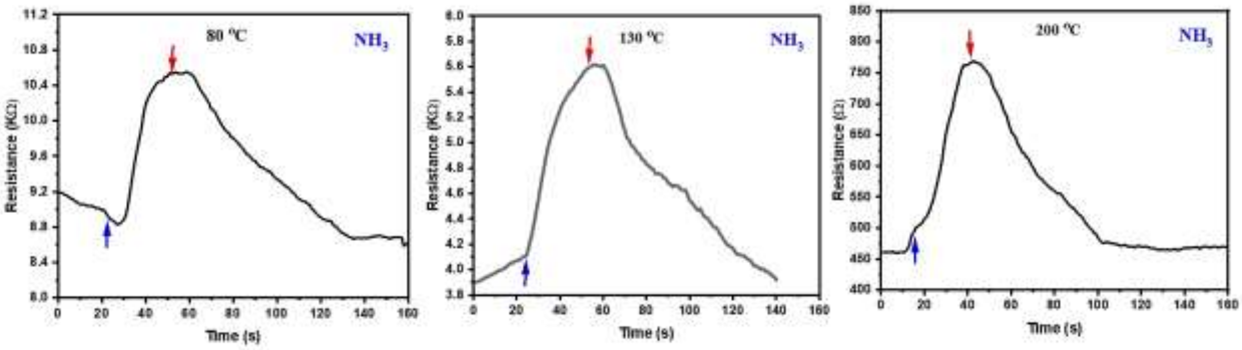

Figure 7. Changes in Ag_2O film resistance to NH_3 gas at various operation temperatures.

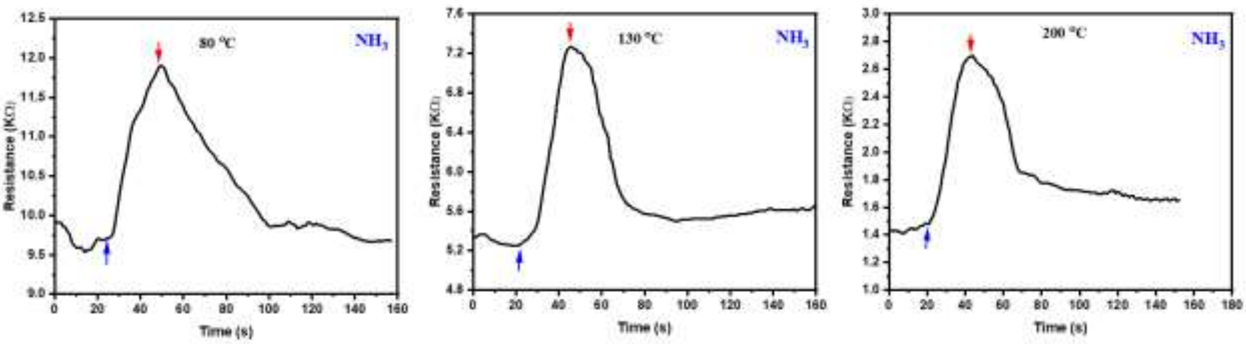

Figure 8. Changes in $(Ag_2O)_{0.8}(SnO_2)_{0.2}$ film resistance to NH_3 gas at various operation temperatures.

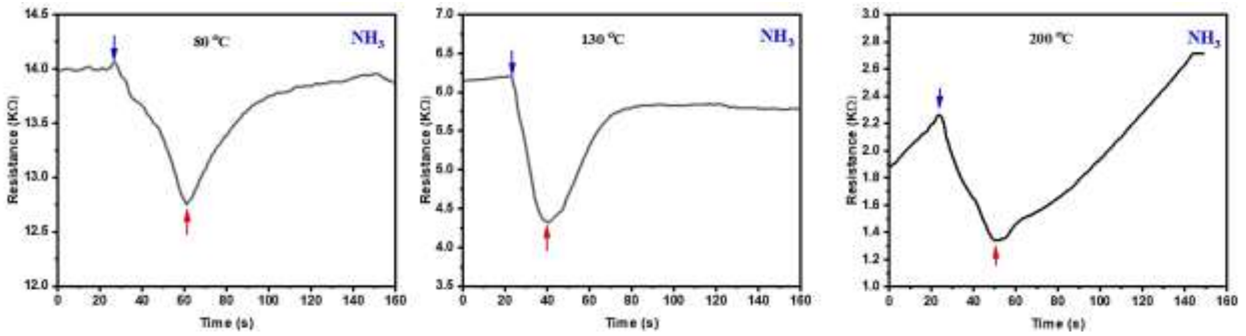

Figure 9. Changes in $(Ag_2O)_{0.6}(SnO_2)_{0.4}$ film resistance to NH_3 gas at various operation temperatures.

2024, 21(4): 1391-1402
https://doi.org/10.21123/bsj.2023.8117
P-ISSN: 2078-8665 - E-ISSN: 2411-7986
Baghdad Science Journal

Table 4 shows the sensitivity, response time, and recovery time for thin films formed of $(Ag_2O)_{1-x}(SnO_2)_x$ against the reducing NH_3 gas at various working temperatures (80, 130, and 200°C). The response and recover times of each sensor to the (95 ppm) NH_3 gas were less than 29.7 seconds and less than 86 seconds, respectively.

Table 3. Sensitivity, response time, and recovery time for $(Ag_2O)_{1-x}(SnO_2)_x$ films toward NH_3 gas at various operating temperatures.

$(Ag_2O)_{1-x}(SnO_2)_x$	Operating. temp.(°C)	NH_3		
		S%	Response time	Recover time
x=0 (Ag_2O)	80	17	24.3	45
	130`	35.5	23.4	44.1
	200	50.5	22.5	39.6
x=0.2	80	22.1	21.6	46.8
	130	38.0	20.7	49.5
	200	78.4	19.8	51.3
x=0.4	80	10.2	34.2	36
	130	46.1	15.3	54
	200	68.6	24.3	45.3

The alteration of NH_3 gas sensitivity with the composite ratio (x) for $(Ag_2O)_{1-x}(SnO_2)_x$ nanocomposite thin films is shown in Fig 10. According to Eranna G.[35] the surface roughness increases as the particle size lowers, increasing the surface area exposed to the gas target. It is also noted from AFM analysis that the surface roughness of $(Ag_2O)_{1-x}(SnO_2)_x$ nanocomposite is greater than the pure Ag_2O, Therefore, the nanocomposite with concentration x=0.2wt has more surface roughness compared to the nanocomposite with concentration x=0.4wt. Furthermore, as-sensing capabilities of $(Ag_2O)_{1-x})$ $SnO_2)_x$ films have been increased compared to pure Ag_2O at x=0.2 and 0.4wt. Additionally, at operating temperatures of 200 °C, the sensitivity achieved its highest values at 78.3% for $(SnO_2)_{1-x}(Ag_2O)_x$ when x=0.2wt. Because it has the roughest surface with the smallest particle size, which has a substantial impact on how gas is sensed[36].

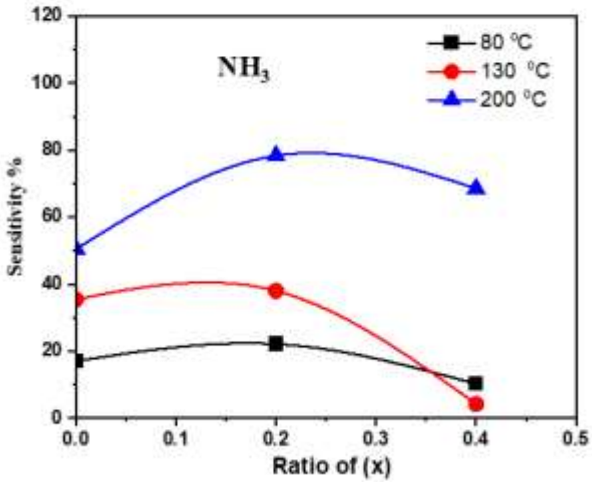

Figure 10. The $(Ag_2O)_{1-x}(SnO_2)_x$ nanocomposite thin films at various operating temperatures as a function of NH_3 gas sensitivity

Conclusion

Ammonia gas sensors based on $(Ag_2O)_{1-x}(SnO_2)_x$ nanocomposites with different ratios of x=0,0.2, and 0.4wt were prepared by the PLD method and their structural, optical and gas sensor properties were characterized. According to the XRD data, the thin film of the $(Ag_2O)_{1-x}(SnO_2)$ nanocomposite has a lattice made up of a mixture of hexagonal Ag_2O and tetragonal SnO_2 structures. An EDX examination revealed the presence of silver, tin, and oxygen in $(Ag_2O)_{1-x}(SnO_2)$, which is how those elements are combined to produce the composites. The quantum confinement effect is responsible for the Ag_2O thin film's absorption edge's blue-shift when compared to its bulk, as seen by the UV-visible spectroscopy. Plus, with x=0,0.2, and 0.4wt, respectively, the obtained energy band gap values of $(Ag_2O)_{1-x}(SnO_2)$thin films are 2.06, 3.24, and 3.36 eV. All film nanoparticles had a spherical shape, as shown by FESEM and AFM analyses. According to AFM analysis, the films' RMS roughness ranged from 4.92 to 8.22 nm and their grain sizes ranged from 37.68 to 49.57 nm. Plus, the thin film prepared at x=0.2wt has the lowest grain size (37.68nm) and maximum RMS roughness (8.22nm), which has a substantial impact on the gas sensitivity of films. Consequently, at 200 ºC, $(Ag_2O)_{0.8}(SnO_2)_{0.2}$ had the maximum sensitivity to NH_3 gas, at 78.4%. When compared to the sensitivity of pure Ag_2O, this sensitivity value is significantly higher.

Acknowledgment

For its laboratory facilities, the authors thank the University of Baghdad's College of Science for Women's Physics Department. We would want to express our gratitude to everyone who contributed with this project in any way.

Authors' Declaration

- Conflicts of Interest: None.
- We hereby confirm that all the Figures and Tables in the manuscript are ours. Furthermore, any Figures and images, that are not ours, have been included with the necessary permission for re-publication, which is attached to the manuscript.
- Ethical Clearance: The project was approved by the local ethical committee in University of Baghdad.

Authors' Contribution Statement

All authors contributed to the completion of this work. N. M. A., preparing the samples and performing the tests. A. A. B. wrote the manuscript, analysis the data and evaluated the information.

References

1. Wang S-Y, Ma J-Y, Li Z-J, Su H, Alkurd N, Zhou W-L, et al. Surface acoustic wave ammonia sensor based on ZnO/SiO2 composite film. J Hazard Mater. 2015; 285: 368-74. https://dx.doi.org/10.1016/j.jhazmat.2014.12.014
2. Wang T, Lu G, editors. Demonstrating the impact of Band Gap Modilation on Semiconductor Metal Oxide Gas-sensing Performance. ECS Meeting Abstracts; 2021; 63: 63. IOP publishing https://dx.doi.org/10.1149/MA2021-01631693mtgabs
3. Nakarungsee P, Srirattanapibul S, Issro C, Tang I-M, Thongmee S. High performance Cr doped ZnO by UV for NH_3 gas sensor. Sens Actuator A Phys. 2020; 314: 112230. https://dx.doi.org/10.1016/j.sna.2020.112230
4. Li P, Wang B, Qin C, Han C, Sun L, Wang Y. Band-gap-tunable CeO_2 nanoparticles for room-temperature NH_3 gas sensors. Ceram Int. 2020; 46(11): 19232-40. https://dx.doi.org/10.1016/j.ceramint.2020.04.261
5. Liu H, Shen W, Chen X, Corriou J-P. A high-performance NH_3 gas sensor based on TiO_2 quantum dot clusters with ppb level detection limit at room temperature. J Mater Sci: Mater Electron. 2018; 29(21): 18380-7. https://dx.doi.org/10.1007/s10854-018-9952-9
6. Kulkarni S, Navale Y, Navale S, Stadler F, Ramgir N, Patil V. Hybrid polyaniline-WO_3 flexible sensor: a room temperature competence towards NH_3 gas. Sens. Actuators B Chem. 2019; 288: 279-88. https://dx.doi.org/10.1016/j.snb.2019.02.094
7. Kareem MM, Kadem BY, Mohammad EJ, Atiyah AJ. Synthesis, Characterization and Gas Sensor Application of New Composite Based on MWCNTs: CoPc: Metal Oxide. Baghdad Sci J. 2021; 18(2): 384. https://dx.doi.org/10.21123/bsj.2021.18.2.0384
8. Bhanjana G, Chaudhary GR, Dilbaghi N, Chauhan M, Kim K-H, Kumar S. Novel electrochemical sensor for mononitrotoluenes using silver oxide quantum dots. Electrochim Acta. 2019; 293: 283-9. https://dx.doi.org/10.1016/j.electacta.2018.10.042
9. Rahman MM, Khan SB, Jamal A, Faisal M, Asiri AM. Highly sensitive methanol chemical sensor based on undoped silver oxide nanoparticles prepared by a solution method. Microchim Acta. 2012; 178(1): 99-106. https://dx.doi.org/10.1007/s00604-012-0817-2
10. Murray B, Li Q, Newberg J, Hemminger J, Penner R. Silver oxide microwires: electrodeposition and observation of reversible resistance modulation upon exposure to ammonia vapor. Chem Mater. 2005; 17(26): 6611-8. https://dx.doi.org/10.1021/cm051647r
11. Jamal RK, Ali FH, Hameed MM, Aadim KA. Designing A zener diode using Ag2O (1-X) Zno (X)/Psi structures deposited by laser induced plasma technique. Iraqi J Sci. 2020: 61(5): 1032-9. https://dx.doi.org/10.24996/ijs.2020.61.5.12

12. Ida Y, Watase S, Shinagawa T, Watanabe M, Chigane M, Inaba M, et al. Direct electrodeposition of 1.46 eV bandgap silver (I) oxide semiconductor films by electrogenerated acid. Chem Mater. 2008; 20(4): 1254-6 https://dx.doi.org/10.1021/cm702865r
13. Saroja G, Vasu V, Nagarani N. Optical Studies of Ag_2O thin film prepared by electron beam evaporation method. Open J Met. 2013; 3(4): 7. https://dx.doi.org/10.4236/ojmetal.2013.34009 .
14. De AK, Sinha I. Synergistic effect of Ni doping and oxygen vacancies on the visible light photocatalytic properties of Ag_2O nanoparticles. J Phys Chem Solids. 2022; 167: 110733. https://dx.doi.org/10.1016/j.jpcs.2022.110733
15. Alwan AM, Yousif AA, Abed HR, editors. High sensitivity and fast response at the room temperature of SnO_2: CuO/PSi nanostructures sandwich configuration NH_3 gas sensor. AIP Conf Proc. 2019; 2190(1): 020086. https://dx.doi.org/10.1063/1.5138572
16. Shaker DS, Abass NK, Ulwall RA. Preparation and study of the Structural, Morphological and Optical properties of pure Tin Oxide Nanoparticle doped with Cu. Baghdad Sci J. 2022; 19(3): 0660-. https://dx.doi.org/10.21123/bsj.2022.19.3.0660
17. Al-Jumaili HS, editor NO_2 gas sensor properties of In_2O_3-CuO Nanocomposite thin films prepared by chemical spray pyrolysis. IOP Conf Ser: Mater Sci Eng; 2021: 1095(1): 012008 https://dx.doi.org/10.1088/1757-899X/1095/1/012008
18. Liang Y-C, Liu Y-C. Design of nanoscaled surface morphology of TiO_2–Ag_2O composite nanorods through sputtering decoration process and their low-concentration NO_2 gas-sensing behaviors. Nanomaterials. 2019; 9(8): 1150. https://dx.doi.org/10.3390/nano9081150
19. Rezaei K, Nasirian S. A low-level acetone gas sensor based on n-type ZnO/p-type CuO composite nanostructure for the diagnosis of diabetes in dynamic situations. J Mater Sci: Mater Electron. 2021; 32(4): 5199-214. https://doi.org/10.1007/s10854-021-05251-8
20. Yang T, Yang Q, Xiao Y, Sun P, Wang Z, Gao Y, et al. A pulse-driven sensor based on ordered mesoporous Ag_2O/SnO_2 with improved H_2S-sensing performance. Sens Actuators B Chem. 2016; 228: 529-38. https://doi.org/10.1016/j.snb.2016.01.065
21. Rizi VS, Sharifianjazi F, Jafarikhorami H, Parvin N, Fard LS, Irani M, et al. Sol–gel derived SnO_2/Ag_2O ceramic nanocomposite for H_2 gas sensing applications. Mater Res Express. 2019; 6(11): 1150g2 https://dx.doi.org/10.1088/2053-1591/ab511e .
22. Liang YC, Hsu Y W. Design of thin-film configuration of SnO2-Ag2O composites for NO_2 gas-sensing applications. Nanotechnol Rev. 2022; 11(1): n1842-53. https://dx.doi.org/10.1515/ntrev-2022-0111
23. Hu X, Zhu Q, Wang X, Kawazoe N, Yang Y. Nonmetal-metal-semiconductor-promoted P/Ag/Ag_2O/Ag $_3$ PO 4/TiO_2 photocatalyst with superior photocatalytic activity and stability. J Mater Chem A. 2015; 3(34): 17858-65. https://dx.doi.org/10.1039/C5TA05153C
24. Agasti S, Dewasi A, Mitra A, editors. Structural and optical properties of pulse laser deposited Ag_2O thin films. AIP Conf Proc; 2018; 1953(1): 060001. https://dx.doi.org/10.1063/1.5032732
25. Amutha T, Rameshbabu M, Muthupandi S, Prabha K. Theoretical comparison of lattice parameter and particle size determination of pure tin oxide nanoparticles from powder X-ray diffraction. Mater Today Proc. 2022; 49: 2624-7. https://dx.doi.org/10.1016/j.matpr.2021.08.044
26. Ambardekar V, Bandyopadhyay PP, Majumder SB. Hydrogen sensing performance of atmospheric plasma sprayed tin dioxide coating. Int J Hydrog Energy. 2019; 44(26): 14092-104. https://dx.doi.org/10.1016/j.ijhydene.2019.04.013
27. Abdelghany A, Abdelrazek E, Rashad D. Impact of in situ preparation of CdS filled PVP nano-composite. Spectrochim Acta A: Mol Biomol. 2014; 130: 302-8. https://dx.doi.org/10.1016/j.saa.2014.04.049
28. Sharma A, Tomar M, Gupta V. SnO_2 thin film sensor with enhanced response for NO_2 gas at lower temperatures. Sens Actuators B Chem. 2011; 156(2): 743-52 https://dx.doi.org/10.1016/j.snb.2011.02.033 .
29. Sonker RK, Sharma A, Shahabuddin M, Tomar M, Gupta V. Low temperature sensing of NO_2 gas using SnO_2-ZnO nanocomposite sensor. Adv Mater Lett. 2013; 4: 196-201. https://dx.doi.org/10.5185/amlett.2012.7390
30. Singh PK, Bishwakarma H, Das AK. Study of annealing effects on Ag_2O nanoparticles generated by electrochemical spark process J Electron. Mater. 2017; 46(10): 5715-27. https://dx.doi.org/10.1007/s11664-017-5614-6
31. Abbas HH, Hasan BA. The Effect of Silver Oxide on the Structural and Optical Properties of ZnO: AgO Thin Films. Iraqi J Sci. 2022: 1526-39. https://dx.doi.org/10.24996/ijs.2022.63.4.13
32. Jamal RK, Mutlak FA, Ibrahim FT, Nayef UM. Synthesis of Ag_2O films by pulsed laser deposited on porous silicon as gas sensor application. Optik. 2020; 218: 164971. https://dx.doi.org/10.1016/j.ijleo.2020.164971
33. Rivers S, Bernhardt G, Wright M, Frankel D, Steeves M, Lad R. Structure, conductivity, and optical absorption of $Ag_{2-x}O$ films. Thin Solid Films. 2007; 515(24):8684-8. https://dx.doi.org/10.1016/j.tsf.2007.03.139
34. Wisitsoraat A, Tuantranont A, Comini E, Sberveglieri G, Wlodarski W. Characterization of n-type and p-type semiconductor gas sensors based on NiO_x doped TiO_2 thin films. Thin Solid Films. 2009; 517(8): 2775-80.
35.Eranna G. Metal oxide nanostructures as gas sensing devices:CRC press; 2011. https://dx.doi.org/10.1016/j.tsf.2008.10.090

2024, 21(4): 1391-1402
https://doi.org/10.21123/bsj.2023.8117
P-ISSN: 2078-8665 - E-ISSN: 2411-7986
Baghdad Science Journal

36. Pravarthana D, Tyagi A, Jagadale T, Prellier W, Aswal D. Highly sensitive and selective H_2S gas sensor based on TiO_2 thin films. Appl Surf Sci. 2021; 549: 149281. https://dx.doi.org/10.1016/j.apsusc.2021.149281

مستشعر غاز NH_3 الانتقائي المرتكز على الأغشية الرقيقة للمركبات النانوية $(Ag_2O)_{1-x}$ $(SnO_2)_x$ عند درجات حرارة تشغيل مختلفة

ندى محمد عباس، انوار علي باقر

قسم الفيزياء، كلية العلوم للبنات، جامعة بغداد، بغداد، العراق .

الخلاصة

تم استخدام تقنية ترسيب الليزر النبضي (PLD) للتحضير الأغشية الرقيقة $(Ag_2O)_{1-x}(SnO_2)_x$ النانوية المركبة بنسب مختلفة من x=(0, 0.2,0.4) من النسب الوزنية المرسبة على قواعد زجاجية. تم تلدين الأفلام بعد ذلك في الهواء لمدة ساعتين عند 300 درجة مئوية. تم تأكيد تشكيل المركب $(Ag_2O)_{1-x}(SnO_2)_x$ من خلال تحقيق حيود الأشعة السينية(XRD). وفقًا للفحص المجهري الإلكتروني الماسح (FESEM) ، كانت جزيئات $(Ag_2O)_{1-x}(SnO_2)_x$ التي تم إنشاؤها كروية الشكل. تم أستخدم تحليل مطياف تشتت الاشعة السينية (EDX) لتأكيد العناصر الموجودة في الأفلام المركبة.اظهر تحليل القوة الذرية المجهري (AFM) أن الأفلام الناتجة لها حجم حبيبي بين 37.68 - 49.57 نانومتر وخشونة متوسط الجذر التربيعي (RMS) من 4.92 إلى 8.22 نانومتر. تحتوي الأفلام المحضرة على فجوة طاقة مباشرة بين 2.06 و 3.36 الكترون فولت ، وفقاً لبيانات المطياف المرئي للأشعة فوق البنفسجية (UV-Vis) . تم اختبار الأفلام لاستشعار NH_3 تحت درجات حرارة تشغيل مختلفة. الاختلافات الملحوظة في مقاومة الغشاء الرقيق لاستجابة استشعار الغاز تدل على الموصلية من النوع n او النوع p عند الغاز المختزل ، تزداد مقاومة أفلام $(Ag_2O)_{1-x}(SnO_2)_x$ عندما تكون x=0, 0.2wt ، مما يشير إلى أن الأفلام من النوع p ، ومع ذلك ، فإن الفيلم الرقيق يعرض السلوك العكسي عندما x = 0.4wt ، مما يشير إلى أنه من النوع n بالإضافة إلى ذلك ، أظهرت جميع الأفلام التي تم إنتاجها حساسية لغاز NH_3 بتركيز 95 جزء في المليون. يمتلك الغشاء الرقيق Ag_2O حساسية بنسبة 50.5٪ عند درجة حرارة تشغيل 200 درجة مئوية مع أوقات استجابة واسترداد تبلغ 22.5 و 39.6 ثانية على التوالي.علاوة على ذلك أظهرت الأغشية الرقيقة المركبة حساسية أكبرمن الأغشية الرقيقة المصنوعة من أوكسيد الفضة النقي.

الكلمات المفتاحية: Ag_2O- SnO_2، المركبات النانوية، مستشعرغاز NH_3، درجات حرارة التشغيل, ترسيب الليزر النبضي.